Sixth International Conference on Durability of Concrete Structures **Paper Number ICC22**
18 - 20 July 2018
University of Leeds, Leeds, West Yorkshire, LS2 9JT, United Kingdom

Comparison of alkali-silica chemical reaction of reactive glass and chert aggregate

Y. Morinaga, E. Yogarajah and T. Nawa
Graduate School of Engineering, Hokkaido University, Sapporo, Hokkaido, Japan

L. Yorgchaitrakul
Construction and Maintenance Technology Research Center (CONTEC), International Institute of Technology (SIIT), Thammasat University, Klong Luang, Pathumthani, Thailand

E. Iwatsuki
Department of Urban Environment Engineering, Aichi Institute of Technology, Yakusa-cho, Aichi, Japan

ABSTRACT

Alkali silica reaction (ASR) is one of the most important factors of deterioration of Concrete. However, there are a lot of unknown points about ASR such as mechanism of ASR and pessimum effect. We investigate to the mechanism of Alkali silica chemical reaction by using two different aggregates, early type expanded aggregate and delayed type expanded aggregate. Experiments were used to investigate ASR by reaction between reactive silica and alkali ions with or without calcium ions. Two phases of reacted samples (liquid and solid) are presented. In the absence of calcium hydroxide (CH), reactive materials with specified sizes (Yoro-chert, and Pyrex glass) were mixed with sodium hydroxide (1M-NaOH) and kept at temperatures of 70°C. After specified reaction times, liquid samples with or without CH were withdrawn, filtrated, and provided for an ICP-AES analysis to investigate the concentration of silica. After the filtration, insoluble product mixed with CH at 70 °C was used to investigate the chemical components and structure using XRD, ^{29}Si-NMR and SEM/EDX. NMR and ICP results show that degree of dissolved SiO_2 from Yo+CH samples is higher than that of PG+CH after 5 days of reaction, but the results are in opposite for the case of without CH. Further, the amount of Q_3 sites, which contributes to expansion, in the ASR products of Yo+CH is lower than that of Pyrex glass, indicating that expansion from ASR cannot be explained by only the reaction degree of aggregates. However, the pH changes in the solution is related to Q^3 sites suggesting that pH around the aggregates significantly affects the expansion.

Keywords: ASR, chemical reaction, Aggregate, Glass, C/S, pH.

1.0 INTRODUCTION

The alkali silica reaction (ASR) in hardened concrete occurs by a chemical reaction of reactive silica in the aggregate with alkali and hydroxide ions in the pore solution to produce hydrous calcium-alkali-silicate and alkali-silicate gels (Ichikawa and Miura, 2007; Hou *et al*. , 2005; Hou *et al*., 2004; Kim and Olek, 2014; Ichikawa 2009; T.Katayama, 2012). These so-called ASR gels absorb water, and the resulting swelling expansion causes cracks in the aggregate grains and in the surrounding cement paste matrix, leading to a loss of strength and reductions in the elastic modulus and durability of the concrete. Consequently, the ASR damages concrete structures, resulting in a shortening of their service life and leading to the generally acknowledged understanding that the ASR is a major liability for the durability of concrete structures.

The expansion process occurs due to the formation of gel by the ASR reaction. The main factors that contribute to the ASR formation are reactive aggregates, highly alkaline conditions, and the moisture content in the pore solution. In particular, the aggregates used have a strong influence on the swelling mechanism generated by the reactions. This is because, with reactive aggregates, free silica is easily dissociated into the pore solution by the activity of OH−. Highly reactive compounds tend to result in increased silica availability for the ASR. It is accepted that the ASR is a chemical reaction that is highly sensitive to temperature (Damgaard Jensen *et al*., 1982; Swamy, 1986). Thus, a rise in temperature may be involved in increases in the dissolution rate of soluble silica. Therefore, more silica available in the pore solution results in greater amounts of the ASR product that in turn may induce expansion by water absorption due to the swelling characteristics of the gel. The swelling of the gel is related to its chemical composition. Garcia-Diaz *et al*. (2006) have proposed

a damage mechanism due to the ASR by detailing a swelling curve divided into 4 periods: (i) The Q^0 ($H_2SiO_4^{2-}$) tetrahedron formed from dissolution, followed by a reaction with alkali and Ca ions, producing Q^0 ($H_2SiO_4^{2-}$) products such as calcium silicate hydrate (C-S-H) and calcium alkali silicate hydrate (C-Na/K-S-H), with no appreciable swelling; (ii) A transition from Q_4 (SiO_2) to Q^3 ($SiO_{5/2}^-$) increases the yield of Q^3 ($SiO_{5/2}^-$) tetrahedra in the aggregate, which is responsible for the swelling and cracking; (iii) The dissolution and precipitation process in period two occurs while Q^0 ($H_2SiO_4^{2-}$) products fill the cracks generated by the swelling; (iv) The swelling is asymptotic and the reaction continues to produce more Q^0 ($H_2SiO_4^{2-}$) and Q^3 ($SiO_{5/2}^-$), further filling the cracks.

It may be deduced that the rate of expansion due to the ASR depends on the contents of the ASR as well as on the capacity available for swelling of the gel. A study to determine the relation of the ASR expansion to the degree of reaction has been reported. The use of scanning electron microscopy (SEM) image analysis (Haha *et al*., 2007)showed that for potentially reactive ASRs, the degree of reaction of the aggregate is around 0.3%. Bulteel *et al*. (2002) developed a chemical method for quantitative characterization of the ASR by considering two reaction degrees: the number of moles generated by siloxane bond break-up inside the aggregate and the number of moles of monomers and small polymers obtained from dissolution. Additionally, the reported activation energy of reactive flint aggregate is approximately 78 kJ/mol (Bulteel *et al*., 2002). This activation energy value is close to the activation energy that breaks siloxane bonds, which would be the limiting step of the dissolution process.

Kawamura *et al*. (2004) revealed that both Pyrex glass and Yoro-chert are deleterious materials that are prone to the ASR problem and, furthermore, mortar with Pyrex glass expanded rapidly when compared with Yoro-chert mortar. The high expansion of Pyrex glass mortar was related to the amount of silica dissolution. Therefore, the rate of dissolution of soluble silica is a key factor in the ASR and is related to the ambient temperature, as higher temperatures may accelerate the ASR, thereby yielding more ASR gel in the pore solution and causing significant expansion. However, few studies have focused on the relationship between the dissolution rate of soluble silica and the gel composition, particularly regarding the difference in the siliceous materials. Our previous study has compared the ASR formation in two different reactive chert aggregates (Baingam *et al*. 2015).

2.0 MATERIALS AND METHODS

2.1 Material and sample preparation

In this study, silica samples made with Pyrex glass (PG) and Yoro-chert (Yo) were used. PG produced by the Iwaki Company was selected as a highly reactive silica, while Yo from Gifu prefecture, Japan, was composed of sedimentary rock having minerals of chalcedony and cryptocrystalline quartz. The ASR behaviours of Yo were tested by the method of JIS A1145 and reported in Baingam *et al.* (2015). Table 1 presents the chemical compositions analysed by X-ray fluorescence. The study aims to obtain basic information on the ASR by characterizing pore solutions and reaction products in the samples for the ASR. The experimental procedure was essentially the same as that of our previous report (Baingam *et al*., 2015). The reaction of aggregates was observed using siliceous aggregates, portlandite (CH), and 1 mol/L NaOH (NH). NH plays the role of the pore solution and CH acts to represent the source of calcium in the actual hardening of mortar and concrete. Before use, the aggregates were ground and sieved to a range of particle sizes from 300 to 150 μm. For the CH conditions, 5 g of aggregate was combined with 1.54 g of CH and then gently mixed. Then, a solution of 1 mol/L NH was added to the samples at an aggregate/solution ratio of 0.25. The samples were then decanted into several 50 mL polyethylene bottles and placed in an oven at 70 °C to accelerate the reactions. The reaction was stopped with 1 mol/L NH at 1, 2, 3, 5, 7, 10, 14, 20 and 24days and samples were filtered through a 0.45-μm filter and washed with acetone to stop the reactions. With the rapidly reacting glass, the reaction was shortened and stopped at 1, 2, 5, 7, 10, 14 and 24days for the PG mixtures. Solids were placed in an oven at 40 °C until fully dehydrated. After the dehydration, the solids were ground to a fine powder (particle sizes smaller than 150 μm) and analysed with X-ray diffraction (XRD), ^{29}Si solid-state nuclear magnetic resonance (NMR), and scanning electron microscopy (SEM) with energy-dispersive X-ray analysis (EDX). After the filtration, liquid samples were prepared for the pore solution analysis. Test samples and exposure parameters are detailed in Table 2.

Table 1. Chemical composition of compounds by X-ray fluorescence spectroscopy

(%)	SiO_2	B_2O_5	Al_2O_3	Na_2O +K_2O	Others
PG	80.9	12.6	2.3	4.0	0
Yo	93.3	0	4.61	0.25	1.84

Table 2. Test samples and exposure parameters to be used in experiments

Reacted samples	1 mol/L NaOH solutions(mL)	CH solid(g)	Aggregate(g)	Exposure conditions(℃)
PG	20	0	5	70
PG+CH		1.54		
Yo		0		
Yo+CH		1.54		

2.2 Experimental methods

Samples were filtrated by a 0.45-μm filter for 1, 2, 3, 5, 7, 10, 14, 20 and 24days and the solids were washed to stop the reactions. Liquid samples were diluted in the range of 10 ppb to 10 ppm of Si concentration and then the dissolved Si content in the liquid samples was quantified by inductively coupled plasma atomic emission spectroscopy (ICP-AES). The chemical composition and structural analyses of the hydrated products were conducted only under a temperature of 70 °C as investigated by XRD, ^{29}Si-NMR, and SEM-EDX. The fine powder for the XRD was analysed using a Rigaku instrument with Cu-KαT radiation ranging from 2θ = 5–70° at a scanning rate of 6.5° per min and a step size of 0.02°.

The ^{29}Si-NMR analysis was performed and recorded by a 9.4-T Bruker MSL 400 operating with a frequency of 79.486 MHz for 29Si at room temperature to show the structure of the produced ASR in the solids. The conditions of the analysis were as follows: a 90° pulse length of 5 μs was used with a ^{29}Si recycling delay of 15 s and 480 scans for the Yo samples, while 15 s and 1920 scans were used for the PG. The external standard was Q_8M_8 ($Si(CH_3)_8Si_8O_2$) at 12.4 ppm for the ^{29}Si-NMR chemical shifts.

The NMR data was transferred to a PC and further explored by the NUT program (Acorn 1997). The data were manually phased and baselines corrected. For SEM/EDX analysis, the powder samples were coated with platinum. The SEM model Super scan SSX-550 combined system with EDX was operated at room temperature using an accelerating voltage at 15.0 kV for the SEM and 20.0 kV for the EDX analysis.

3.0 RESULTS AND DISCUSSION

3.1 Experimental results on ionic concentration in liquid samples

The considerable contents of soluble silica (SiO_2) in the Yo and PG samples up to 24 days are shown in Fig. 1. The results suggest that these kinds of rapidly reacting siliceous materials are very sensitive to hydroxide in the solution, and this contributes to the presence of the very high content of soluble silica in the liquid sample within a short period of the start of the process. The figure also shows the content of Si ions in the presence of CH. With CH, there were low contents of Si ions in solutions, which was quite different from the dissolved Si in liquid samples without CH. These changes don't mean that the rate of SiO_2 dissolution is decreasing in presence of $Ca(OH)_2$. Si ions is consumed by the formation of C-(N-)S-H.

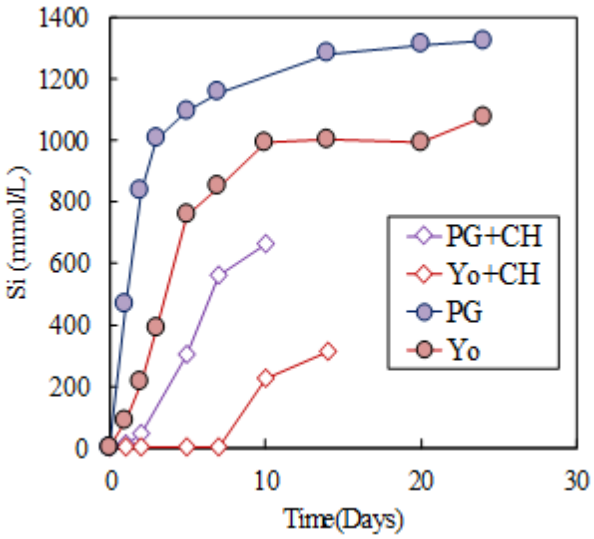

Fig. 1. The concentration of Si ions from Yoro-chert and Pyrex glass at 70℃

At the initial stage, dissolved hydrous silicate ions such as $Si(OH)_2^{2-}$ may react with Ca ions and result in the formation of C-S-H which does not have a constant composition; rather, the composition depends on the activity of the Ca ions. These results suggest that after most of the Ca ions are consumed, the rate of Si dissolution increases. The reaction of PG at 70℃ with or without CH is higher than that which is observed in Yo. The pH of the liquid samples for both Yo and PG at 70℃ is shown in Fig. 2. It is decreasing with reaction time and the pH of the dissolved PG solution is lower than that of the Yo solutions. In addition, the addition of portlandite gave the result that the pH became lower as compared with that without addition. It is conceivable that addition of portlandite produces C-(N-)S-H, resulting in a higher pH at which it is in equilibrium with the solution.

3.2 Solid phases assemblage analysed by XRD, ^{29}Si MAS NMR and SEM/EDX

As detailed above, the C-S-H formation can be attributed to the ASR occurring between the available SiO_2 and Ca ions. For simplicity, the Yo and PG samples under a temperature of 70 °C were selected to further analyse the insoluble product.

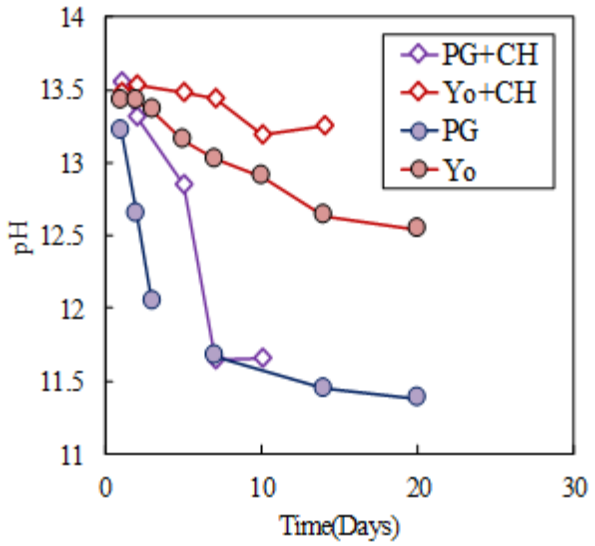

Fig. 2. The pH value of the liquid samples at 70°C

XRD

XRD patterns indicate that Yo and PG consist of quartz and amorphous silica, respectively (Fig. 3(A) and (B)).Furthermore, the figures show that the reaction of both Yo and PG with NaOH does not change their mineralogy. However, the XRD patterns of Yo+CH and PG+CH at 29.4° (2θ) became sharper with the progression of the reaction (Fig. 3(C) and (D)). The peaks also exhibited the diffraction at 7.2° (2θ) that is ordinarily observed with amorphous or disordered crystalline silicate. These peak locations are attributed to Calcium silicate hydrate. (Hou *et al*., 2005; Hou *et al*., 2004). The intensities of the portlandite peaks at 18.0° (2θ) and 34.2° (2θ) decrease with increasing reaction time. The portlandite in the PG+CH and Yo+CH samples completely disappeared after 7days of reaction.

^{29}Si MAS NMR

NMR spectra of the original Yo consist of Q^4 sites only, but PG has both Q^3 and Q^4 sites, as shown in Fig. 4. Since the proportions of Q^3site and Q^4site of Pyrex glass were 7.8 and 92.2% respectively, the mol (%) of PG was defined as $Q^4 \times (1.078)$ and the Q^3 site amount was defined as $Q^3 - Q^4 \times (0.078)$. Q^1 and Q^2 sites were not detected with the reaction of both samples in the NaOH environment. NMR spectra of PG, no portlandite system, at 24days were changed slightly to those of the original sample. The spectra of the Q^3 site (with 1 OH^-) suggests that the Si-site tetrahedron has three bridging oxygens and one non-bridging oxygen, in which the non-bridging oxygen could be bonded to either OH^-, demonstrating the conversion of the site from Q^4 to Q^3 by Si dissolution. NMR spectra of the Yo specimen at 24days also detected an ASR product signal of Q^3. The spectra of PG+CH curing for 24days at 70℃ were enormously

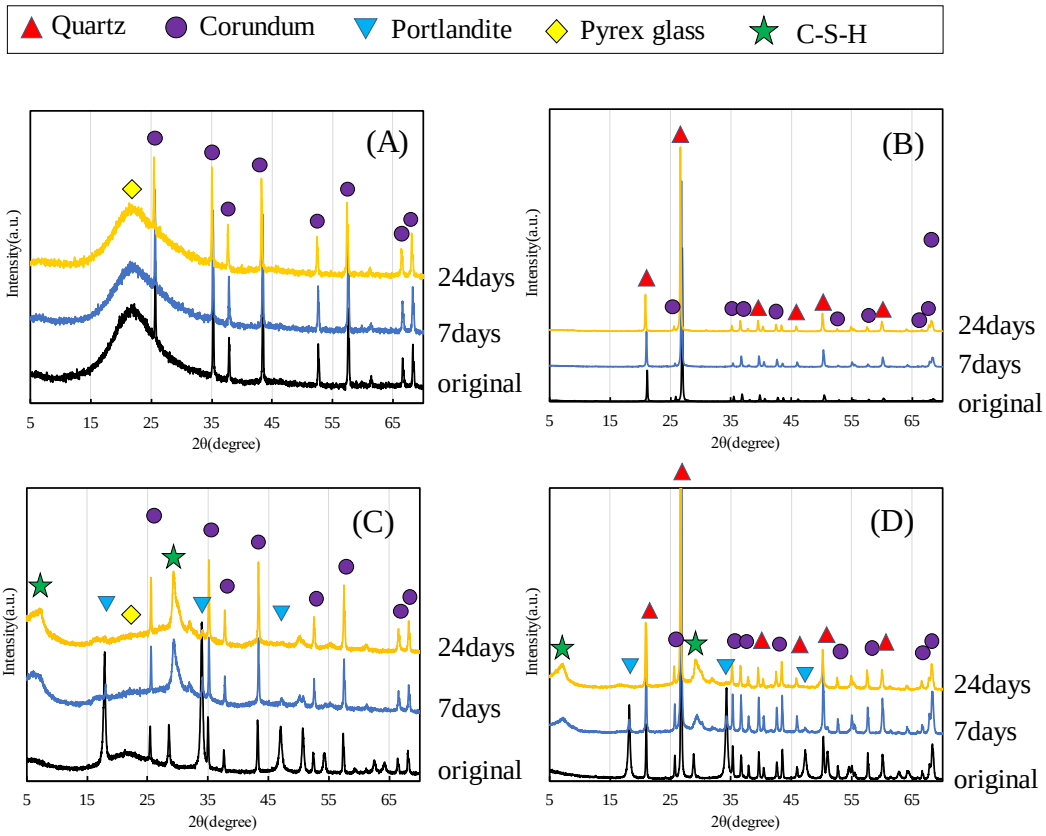

Fig. 3. The XRD pattern for (A)PG, (B)Yo, (C)PG+CH and (D)Yo+CH

changing from the original sample comparing with PG sample curing for 24days. The sites of Q^2, and Q^3 were detected in the samples of PG+CH curing for 24days as shown in Fig. 4(A). The spectra of the Yo+CH samples curing curing for 24days also changing from that of the original Yo sample.

However, the spectra of Yo+CH samples for 24days consists of Q^1, Q^2 and Q^3. It indicates that the proportion of Q^1, Q^2 and Q^3 is different between Yo+CH and PG+CH samples from the results of the deconvolution as shown in Fig. 5. Furthermore, the fraction of Q^n sites in Yo is different from that in PG in presence of CH. For the Yo+CH sample, there are main signals at −78.8 ppm (the end-chain tetrahedral Q^1) and −84.1 ppm (the non-bridging tetrahedral Q^2). This observed spectrum of Q^1 and Q^2 can be related to the ASR product, like C-S-H.

Later in the experiments, the intensity of Q^2 became dominant due to the action of available Ca ions which could be assigned to a more polymerized a defect when compared with the tobermorite structure at a low Ca/Si ratio (Brunet *et al*., 2004; Leemann *et al*., 2011), indicating the structure of C-S-H (Fig. 6). The Q^3 site is precipitation of C-S-H incorporate with Na ions, likely to a C-N-S-H gel with a high silica mean chain length (MCL) (Beaudoin *et al*., 2009). It is accepted that the long MCL of the gel structure has a potential for swelling.

In PG+CH samples, the signal of Q^1 cannot detect except the sample curing for 1hour. Therefore, it was considered that Si chain length of ASR product of PG+CH samples are longer than that of Yo+CH samples. As a result of degree of SiO_2 dissolved comparing with PG, PG+CH, Yo and Yo+CH obtained from the results of ICP-AES and ^{29}Si MAS NMR, reaction rate was increasing in presence of CH regardless of aggregate species. Degree of Si dissolved of Yo chert is lower than that of Pyrex glass without CH addition. However, Yo chert is higher than that of Pyrex glass in presence of CH. On the other hand, the fraction of Q^3, relevant to expansion of mortal, of Yo+CH are lower than that of PG+CH as shown in Fig. 7.

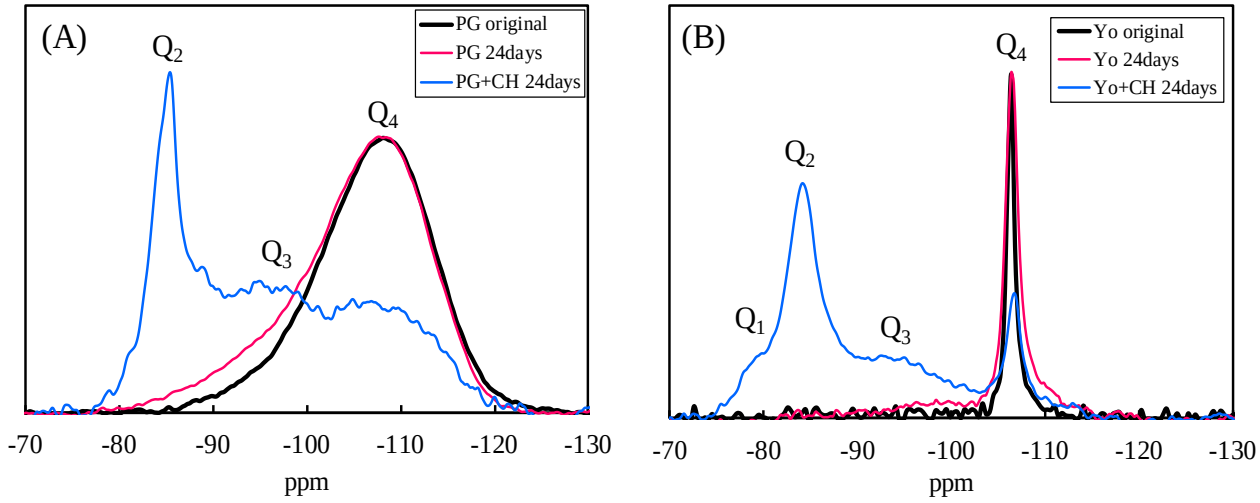

Fig. 4. Comparison of ^{29}Si MAS NMR spectra for original aggregate with that for the sample curing 24days

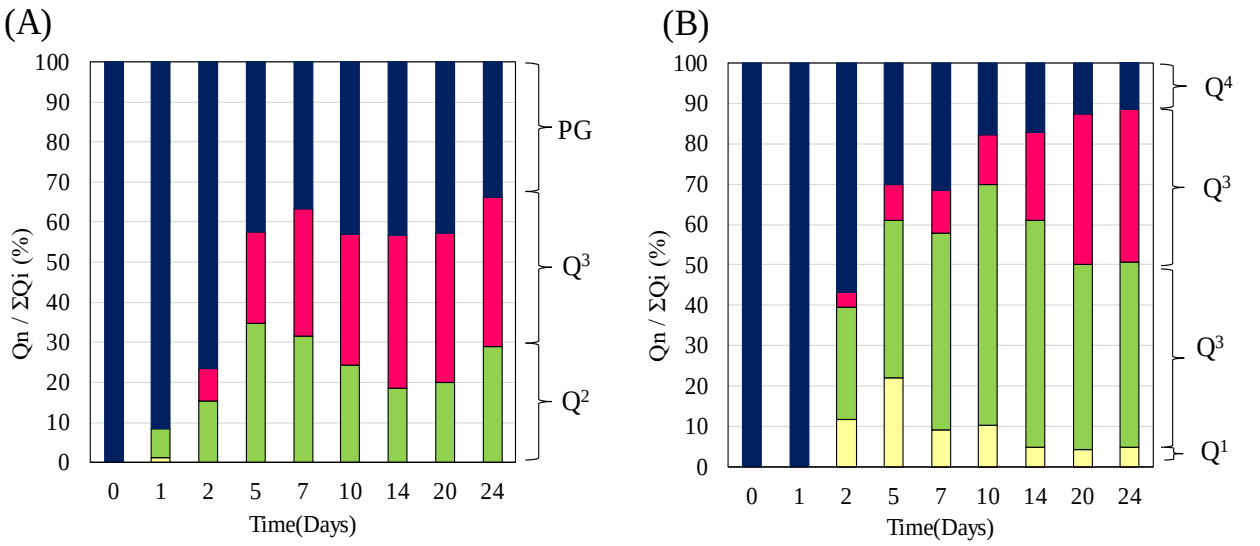

Fig. 5. Propotions of Q^n sites in PG+CH(A) and Yo+CH(B)

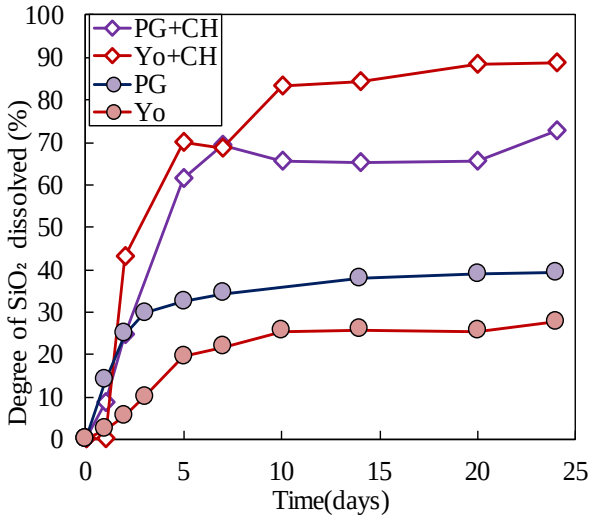

Fig. 6. Degree of SiO_2 dissolution vs time of PG, Yo,PG+CH and Yo+CH

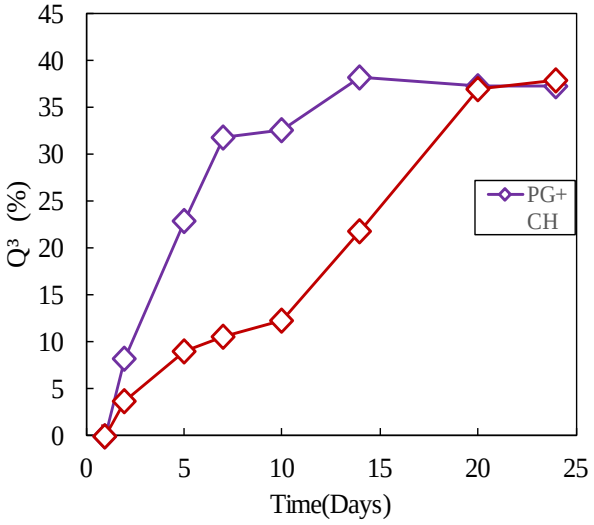

Fig. 7. Proportions of Q^3 sites in PG+CH and Yo+CH

These results indicate expansion behaviour is relation to the proportion of Q^3 because generation of Q^3 of Yo chert, delayed expansion type, is more late than that of Pyrex glass as it was reported in previous study (Garcia-Diaz *et al*., 2006).

SEM/EDX

In this part of the study, Yo+CH and PG+CH (70 °C) were observed by SEM/EDX to quantify the composition of C-N-S-H. A component diagram for C-N-S-H is represented using a triangular shown in Fig. 8. It was suggested that the transition of composition of Ca, Na and Si varies greatly between Yo+CH and PG+CH.

As for sample of PG+CH and Yo+CH, CaO/SiO_2 (C/S) and Na_2O/SiO_2 (N/S) ratios decrease with reaction time. In the case of PG+CH samples, it can be seen that there are two types of ASR products for the reaction from 52 h to 120 h, one having high Ca and Na components, and another having low Ca, although there is a broad distribution of C/S and N/S, and Na components. On the other hand, YO+CH samples cannot show a tendency like PG+CH. Rate of decreasing C/S of YO+CH samples is smaller than that of PG+CH samples as shown in Fig. 9. Furthermore, C/S of Yo+CH samples are higher than that of PG+CH samples after convergence of C/S but there is not quite difference of both aggregate.

Only one ASR product is formed after 120 h of reaction. Kim *et al*. proposed that the ASR in a closed system can be divided into four stages. C-S-H is formed at the beginning, and then the reaction between the existing C-S-H and the alkali and silica ions in the solution forms C-N-S-H. After completion of C-N-S-H formation, the silica concentration in the solution increases and starts to form N-S-H. This could be possible at low concentration of NaOH solution. In this experimental study, C-N-S-H formation is detected as the first product for the PG+CH system, followed by N-S-H formation.

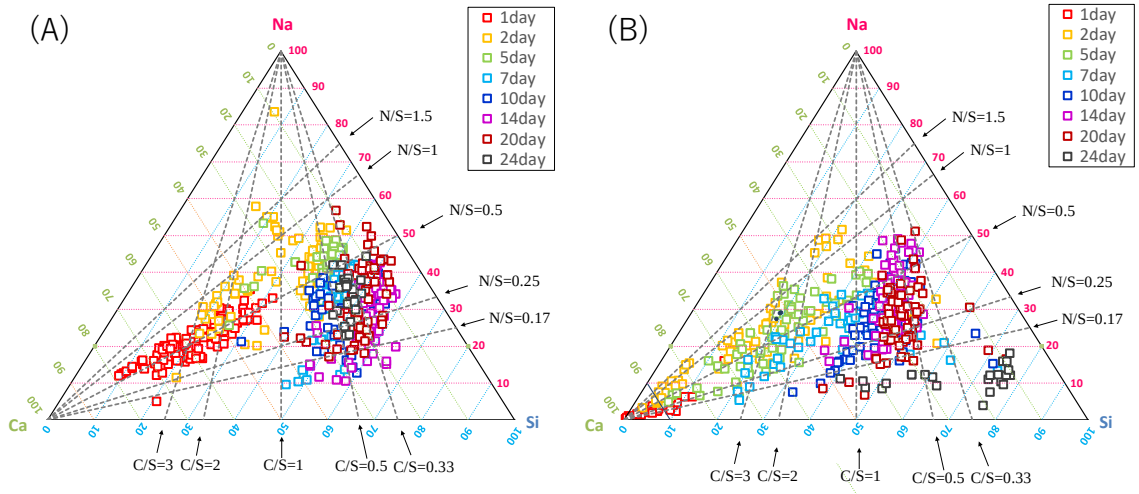

Fig. 8. Triangular components (Ca, Na, Si) diagram showing the representation of mole fraction of C-N-S-H systems. Broken lines indicate different CaO/SiO_2 and Na_2O/SiO_2 ratios

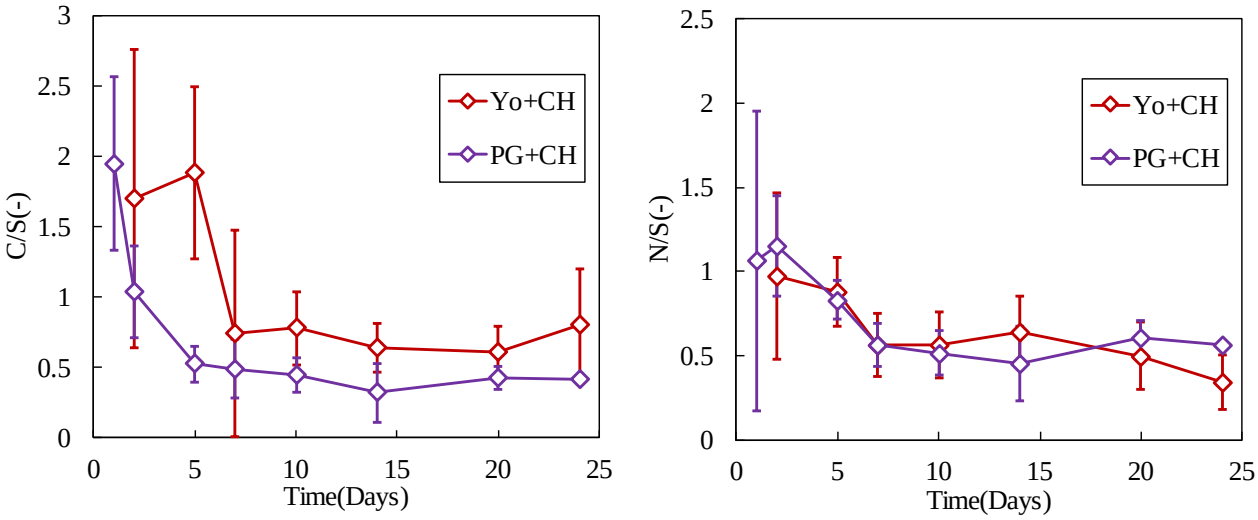

Fig. 9. C/S(Left) and N/S ratios of C-N-S-H systems for PG+CH and Yo+CH

Although C-S-H was not observed as the initial ASR product, the processes of the formation of C-N-S-H and N-S-H agree with the mechanism proposed by Kim *et al.* (2014).

3.3 Factors affecting the formation of Q^3

As explained previously, the amount of Q^3 calculated from ^{29} Si MAS NMR results is highly related to the expansion in ASR. Therefore, in here, key factors affecting the amount of Q^3 in early reactive aggregate (Pyrex glass) and delayed aggregate (Yo chert) are studied. Figure 10 shows the relationship between reaction rate of SiO_2 (aggregate) and the ratio of Q^3. In both types of aggregates, the tendency is same: the amount of Q^3 is increased with the degree of SiO_2 dissolved and then reached to constant after 10% of SiO_2 reaction.

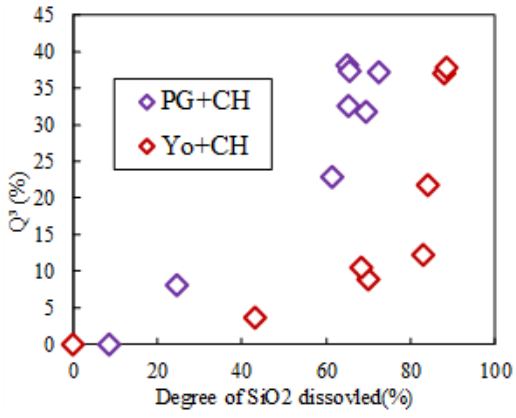

Fig. 10. Relation between Degree of SiO_2 dissolved and proportion of Q^3 sites (%)

However, the amount of Q^3 sites depends on the types of aggregates, and thus, the amount of Q^3, which is an index for expansion in ASR, cannot be evaluated by the reaction rate. Figure 11 shows the relationship between pH and amount of Q^3. The amount of Q^3 increases with decreasing pH and it does not depend on the type of aggregates. Further, the pH influences the composition of ASR products (Fig. 12). This figure indicates that the polymerisation of silica progresses with decreasing of pH. Therefore, it can be inferred that pH around the aggregates significantly affect the formation of Q^3 and thus, expansion due to ASR.

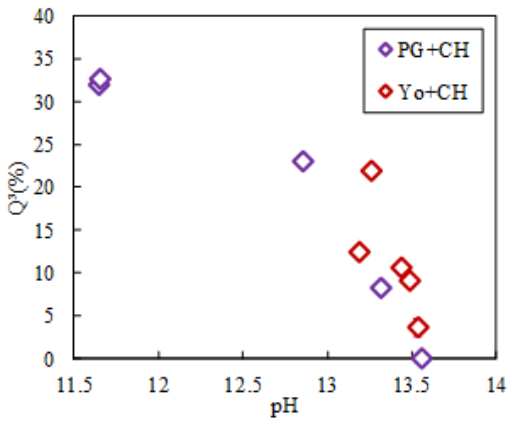

Fig. 11. Relation between pH and proportions of Q^3 sites (%)

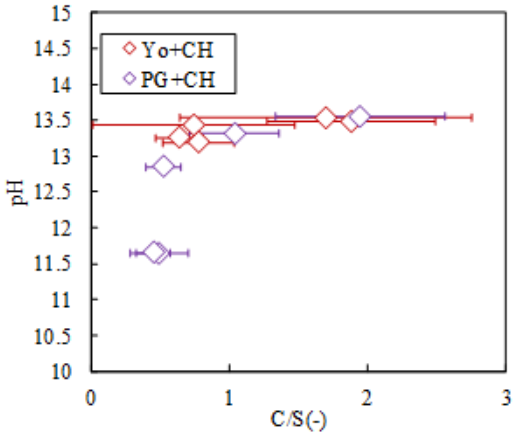

Fig. 12. Relation between pH and proportions of C/S of C-N-S-H systems

4.0 CONCLUSIONS

This study offers one of the factor of deterioration by ASR product formation found in deteriorated concrete subject to the ASR. Although the reactivity of the aggregate to the alkali solution is higher in the early type aggregate, it is obvious that the reaction rate of the delayed expansion type aggregate increases in addition to the increase in the reaction rate as compared with the non-additive system due to the addition of CH. It was revealed that the increased amount of Q3 was delayed in the delay type aggregate as compared with the early type aggregate and it became clear that the expansion timing was delayed unless Q3 was generated even if the aggregate reacted. It was revealed that pH contributed to the production amount of Q3 regardless of aggregate species

References

Acorn, 1997. NUTS-utility transform software 1D version.

Baingam, L. *et al*., 2015. ASR formation of reactive chert in conducting model experiments at highly alkaline and temperature conditions. Construction and Building Materials, 95 :820-831.

Beaudoin, J.J., Raki, L. , Alizadeh, R., 2009. A ^{29}Si MAS NMR study of modified C-S-H nanostructures. Cement and Concrete Composites, 31(8):585–590

Brunet, F. *et al*., 2004. Application of ^{29}si homonuclear and^{1}H-^{29}si heteronuclear nmr correlation to structural studies of calcium silicate hydrates. Journal of Physical Chemistry B, 108(40);15494–15502.

Bulteel, D. *et al*., 2002. Alkali-silica reaction - A method to quantify the reaction degree. Cement and Concrete Research, 32(8); 1199–1206.

Damgaard J, A. *et al*., 1982. Studies of alkali-silica reaction - part I a comparison of two accelerated test methods. Cement and Concrete Research, 12(5), pp.641–647.

Garcia-Diaz, E. *et al*., 2006. Mechanism of damage for the alkali-silica reaction. Cement and Concrete Research, 36(2); 395–400.

Haha, M. Ben *et al*., 2007. Relation of expansion due to alkali silica reaction to the degree of reaction measured by SEM image analysis. Cement and Concrete Research, 37(8); 1206–1214.

Hou, X. *et al*., 2005. Structural investigations of alkali silicate gels. Journal of the American Ceramic Society, 88(4);943–949.

Hou, X., Struble, L.J. & Kirkpatrick, R.J., 2004. Formation of ASR gel and the roles of C-S-H and portlandite. Cement and Concrete Research, 34(9);1683–1696.

Ichikawa, T., 2009. Alkali-silica reaction, pessimum effects and pozzolanic effect. Cement and Concrete Research, 39(8);716–726.

Ichikawa, T. , Miura, M., 2007. Modified model of alkali-silica reaction. Cement and Concrete Research, 37(9);1291–1297.

Kawamura, M. , Iwahori, K., 2004. ASR gel composition and expansive pressure in mortars under restraint. Cement and Concrete Composites, 26(1);47–56.

Kim, T. , Olek, J., 2014. Chemical sequence and kinetics of alkali-silica reaction part II. A thermodynamic model. Journal of the American Ceramic Society, 97(7);2204–2212.

Leemann, A. *et al*., 2011. Alkali-Silica reaction: The Influence of calcium on silica dissolution and the formation of reaction products. Journal of the American Ceramic Society, 94(4);1243–1249.

Swamy, N R., 1986. Influence of Alkali silica reaction on the Engineering properties of concrete. Alkalies in concrete; pp.69–86.

T.Katayama, 2012. Late-expansive ASR in 30year old PC structure in eastern Japan. Proceedings of 14th ICAAR.